

See discussions, stats, and author profiles for this publication at: <https://www.researchgate.net/publication/275242451>

Impact of Moisture Adsorption on Structure and Physical Properties of Amorphous Biopolymers

ARTICLE *in* MACROMOLECULES · APRIL 2015

Impact Factor: 5.8 · DOI: 10.1021/acs.macromol.5b00248

CITATIONS

5

READS

75

5 AUTHORS, INCLUDING:



[Robert Guyer](#)

Los Alamos National Laboratory

249 PUBLICATIONS 4,574 CITATIONS

[SEE PROFILE](#)



[Sinan Keten](#)

Northwestern University

75 PUBLICATIONS 1,471 CITATIONS

[SEE PROFILE](#)



[Dominique Derome](#)

Empa - Swiss Federal Laboratories for Materi...

127 PUBLICATIONS 683 CITATIONS

[SEE PROFILE](#)



[Jan Carmeliet](#)

ETH Zurich

329 PUBLICATIONS 4,806 CITATIONS

[SEE PROFILE](#)

Impact of Moisture Adsorption on Structure and Physical Properties of Amorphous Biopolymers

Karol Kulasinski,^{*,†} Robert Guyer,^{‡,§} Sinan Keten,^{||} Dominique Derome,[⊥] and Jan Carmeliet^{†,⊥}

[†]Chair of Building Physics, Swiss Federal University of Technology Zurich, Stefano-Francini-Platz 5, 8093 Zürich, Switzerland

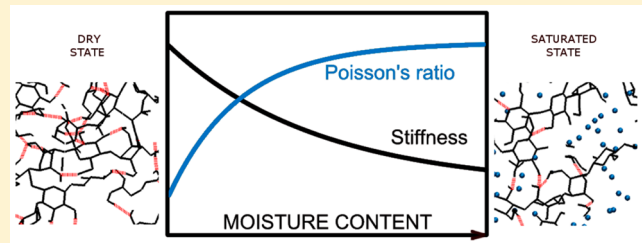
[‡]Solid Earth Geophysics Group, Los Alamos National Laboratory, MS D446, Los Alamos, New Mexico 87545, United States

[§]Department of Physics, University of Nevada, Reno, Nevada 89557, United States

^{||}Department of Civil and Environmental Engineering, Department of Mechanical Engineering, Northwestern University, 2145 Sheridan Road, Evanston, Illinois 60208-3109, United States

[⊥]Laboratory for Multiscale Studies in Building Physics, Empa, Swiss Federal Laboratories for Materials Science and Technology, Überlandstrasse 129, 8600 Dübendorf, Switzerland

ABSTRACT: The interaction of water with many biopolymers is known to rearrange their internal structure, make them moisture sensitive, and influence their physical properties. We study amorphous cellulose and hemicellulose, two hydrophilic biopolymers, using molecular dynamics simulations, and we analyze their structural and physical properties over the full range of moisture content. We find a quasi-linear dependence of volumetric strain on moisture content, and a linear scaling between volumetric strain and porosity, showing that swelling is directly related to the space created by adsorbed water molecules. The interaction of water with the polymer structure results in a weakening of the mechanical properties, leading to rubberlike behavior at high moisture content. Weakening is caused by a decrease in the number of hydrogen bonds that follow exponential scaling. Breaking of the hydrogen bonds system is found to control not only the mechanical response but also the evolution of porosity and the volumetric strain.



INTRODUCTION

Because of their abundance and often unusual properties, biopolymers are intensely studied by researchers and engineers.¹ Among biopolymers, cellulosic materials, cellulose being the most common polymer on earth² and characterized by outstanding mechanical properties (high elastic modulus³), are of particular interest.

The two biopolymers that we study in this paper are amorphous cellulose (AC) and galactoglucomannan, an example of hemicellulose (HC). Both polymers are present in large quantities in wood tracheids, being a part of the S2 layer structure of a wood cell wall. Typically, in softwood, the S2 layer comprises 50% cellulose, 18% glucomannan, 7% xylan (another hemicellulose), 22% lignin, and 3% minor constituents. The cellulose component of the S2 layer has a varying amount of crystalline cellulose and amorphous cellulose; e.g., 40–60% of the cellulose in softwood tracheid cells is amorphous.^{4,5}

Amorphous cellulose is a linear chain of 1- β -linked glucose (Figure 1a) with particularly high aspect ratio, as the degree of polymerization reaches 10^4 units per chain.⁶ Amorphous cellulose (also called paracrystalline cellulose) can be found on the surface of a microfibril, at the interface between crystalline cellulose and hemicellulose.^{7,8} Galactoglucomannan has a backbone built of mannose and glucose residues (Figure 1b), with a ratio of 4:1.^{9–11} The backbone is branched with

galactose (in 8 mass %) linked to mannose, and the backbone residues are acetylated.¹¹ In contrast to cellulose, galactoglucomannan, with degree of polymerization of 10^2 backbone units,¹² forms short chains. Galactoglucomannan is found in the space separating cellulose microfibrils in a fibril aggregate.⁸

Amorphous cellulose and hemicellulose are strongly hydrophilic due to their open porous structure and the presence of exposed hydroxyl (O2 and O3) and hydroxymethyl (O6) groups (Figure 1).^{13,14} Water molecules easily form hydrogen bonds with the oxygen atoms¹⁵ labeled in Figure 1a,b. The adsorption of water influences the mechanical properties of wood polymers^{16,17} primarily due to structural rearrangement and the screening of interactions, i.e., Coulomb and van der Waals forces.^{15,18} The adsorption of water causes an increase in the ability of wood to transport water.^{19–22} The swelling and mechanical properties of AC and HC are the target of the investigation we undertake.

As the adsorption process is an atomic-scale process, force field based molecular dynamics (MD) simulations are an appropriate tool for its investigation. In contrast to mesoscale methods, such as coarse grain, force field based MD can capture hydrogen bonds formation, and unlike more detailed electronic

Received: February 4, 2015

Revised: March 24, 2015

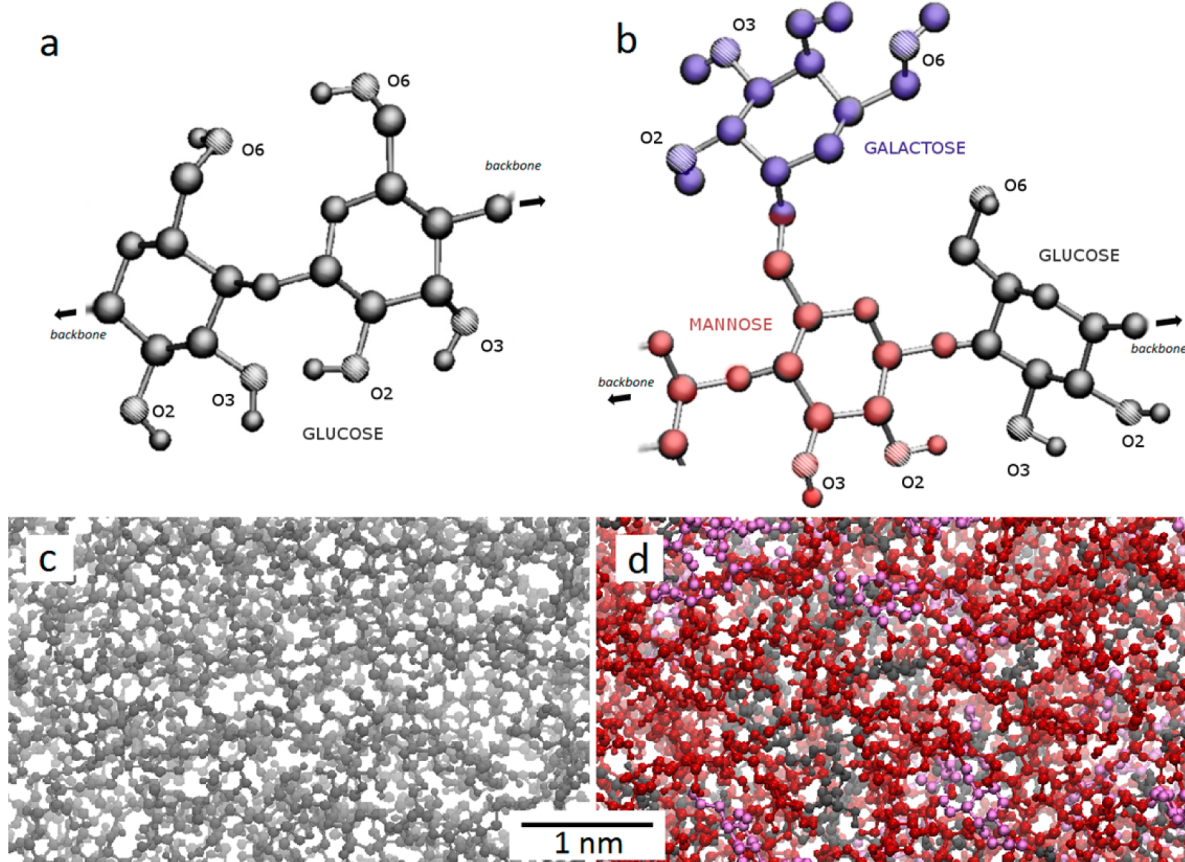


Figure 1. Representation of a chain fragment of (a) amorphous cellulose and (b) galactoglucomannan with united-atom MD where aliphatic hydrogen and its carbon are represented as one bead. The oxygen atoms forming hydrogen bonds with water, O₂, O₃, and O₆, are labeled next to their positions. MD structures of amorphous cellulose (c) and hemicellulose (d) showing random arrangement of chains and the difference in their composition: glucose (gray), mannose (red), and galactose (purple).

structure based methods (e.g., DFT), classical MD enables simulation of larger structures and at longer time scales. Crystalline cellulose has been widely studied with MD simulations.^{23–31} Amorphous cellulose and hemicellulose, apart from xylan, are rarely studied with MD.^{23,32–34}

We investigate in detail the process of water adsorption in AC and HC from the dry state to saturation. We examine the structural changes brought about by adsorption with the aim of understanding how these changes impact the swelling and mechanical behavior of AC and HC. This understanding will aid in developing a picture of moisture behavior of more complex structures, such as a plant cell wall.^{35,36}

MATERIALS AND METHODS

Simulation Details. The molecular dynamics simulations are carried out using Gromacs 4.6 software³⁷ with leapfrog algorithm for integration of Newton's equations of motion and the Gromos 53a6 force field.^{38,39} The cutoff radii of the interactions between atoms are set to 1 nm, the long-range electrostatic interactions are implemented with particle-mesh Ewald summation, the energy and pressure are corrected for dispersion forces, and the distance between oxygen and hydrogen in OH bonds is constrained. Temperature and pressure are controlled by a velocity-rescaling thermostat⁴⁰ and an anisotropic Berendsen barostat,⁴¹ respectively. The simulations are integrated with a time step of 1 fs, and periodic boundary conditions are applied in all directions. Prior to relaxation runs, the systems are energy-minimized with steepest-descent and then conjugated-gradient algorithms. All the measurements are carried out at a constant temperature of 300 K and at constant pressure.

Preparation of Dry Polymers. The model of dry amorphous cellulose contains three chains, each consisting of 60 glucose units or 180 glucose residues in total (Figure 1c). The sample volume and density of dry AC are 36.6 nm³ and 1.33 g/cm³, respectively. The initial configuration of 1 β cellulose was constructed using the “Cellulose-builder” tool.⁴²

The model of dry galactoglucomannan contains 4 chains, each consisting of 100 backbone sugar units (Figure 1d). The model chains have 320 mannose, 80 glucose, and 32 galactose residues. The backbone is built by mannose and glucose units, whereas the galactose is branched to mannose units and the degree of branching is 8%. For the sake of simplicity, the HC chains are not acetylated as the number of acetylated sugars is negligible.¹¹ The degree of polymerization and the 4:1:0.4 ratio of mannose:glucose:galactose are those of softwood and are experiment-based.^{6,10} The sample volume and density of dry HC are 95.1 nm³ and 1.22 g/cm³, respectively. The initial configuration is constructed using Materials Studio software in order to optimize the geometry of single chains.

The procedure of amorphization, described previously,⁴³ has two stages. First, the polymer is raised to temperature 700 K and equilibrated there in stress-free conditions until the chains lose their ordered structure, typically after 1 ns. Then the amorphized chains are quenched to a temperature of 300 K and equilibrated there for 10 ns. Figure 1c,d illustrates the MD structure of amorphous cellulose and hemicellulose.

Water Adsorption. In order to study the response of the polymers to moisture, simple point-charge water molecules⁴⁴ are introduced into the system using the algorithm described in ref 15 and shown schematically in Figure 2a. Starting from the dry system, water molecules are inserted one by one into the void space between the polymer chains. Successful insertion of a water molecule is followed by

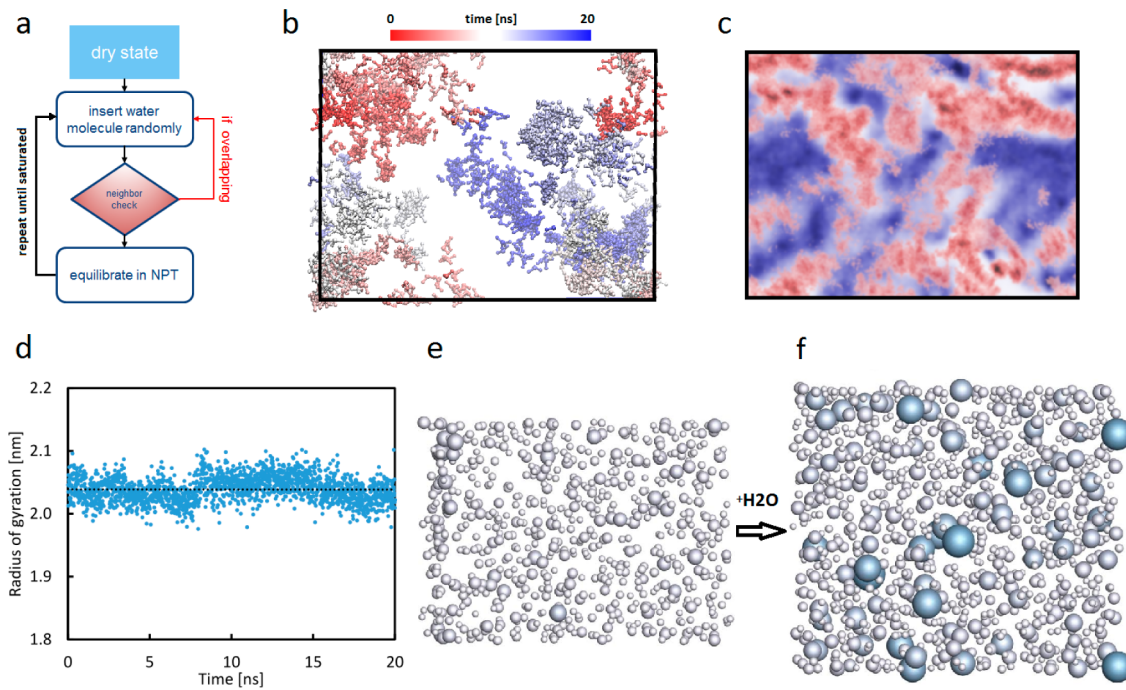


Figure 2. (a) Procedure to mimic moisture adsorption. (b) Trajectory of a single water molecule during 20 ns at $m = 50\%$. During 20 ns the molecule visits a large fraction of the system; the colors blue/white/red mark the evolution of time. (c) 0.3 nm thick cross section of amorphous cellulose at saturation showing the density profile averaged over 20 ns trajectory. Cellulose chains are tinted in red and water molecules in blue, and darker color denotes regions of space more likely to be occupied. White space is not visited. A uniform water distribution means flat potential energy landscape for a water molecule. (d) Fluctuation of the radius of gyration of AC. Representation of porosity of AC in dry (e) and saturated (f) states.

a relaxation run of 10 ps at stress-free conditions. Once the desired number of water molecules has been inserted, relaxation runs of 1 ns and production runs of 20 ns are carried out. The system is characterized by a moisture content value

$$m = \frac{N_{H_2O} M_{H_2O}}{M_{\text{polymer}}^{\text{dry}}} \quad (1)$$

where N_{H_2O} is the number of water molecules in the system, M_{H_2O} is the mass of a water molecule, and $M_{\text{polymer}}^{\text{dry}}$ is the mass of the polymer in dry state. The maximum moisture content ($m = 0.5$) investigated is taken from experiment.⁴⁵

We remark that the preferential use of pure MD simulations instead of the Monte Carlo approach is due to the small volume of void space as compared to the total volume of the system. Monte Carlo insertions, when applied to a high-density system such as cellulose, are inefficient and lead to an elevated rejection rate. Therefore, in order to compensate for the undersampling of MD, we use a sufficiently long simulation time. This condition is satisfied when, during simulation period, water molecules can visit many pores of the system and form hydrogen bonds with a large number of different sorption sites. Figure 2b shows the trajectory of a single water molecule during 20 ns at $m = 0.5$. We observe that during 20 ns the molecule visits a large fraction of the system. We also note that, during the simulation, the radius of gyration is fluctuating around an average value (Figure 2d). We conclude that our MD approach is sufficiently accurate to model the sorption process.

Swelling and Porosity Measurements. As a result of the moisture sorption the system swells. The free volumetric strain, ε_V , at $\sigma_x = \sigma_y = \sigma_z = 0$ is found from

$$\varepsilon_V(m) = \frac{V(m, 0) - V(0, 0)}{V(0, 0)} \quad (2)$$

where $V(m, \sigma)$ is the volume at moisture content m and bulk stress σ .

To determine the porosity, we use a procedure based on the insertion of probe spheres into the polymeric system, in a state frozen

and depleted of its water molecules. We start with a probe sphere of radius $r_{\max} = 1.0$ nm and attempt $N = 10^5$ times to insert this sphere at random locations, such that the sphere does not overlap with van der Waals spheres of the polymer atoms and any already inserted spheres. Each successful insertion is a contribution to porosity. After N attempts, the radius of the probe sphere is decreased by 0.05 nm, and N further insertions are attempted. This procedure is carried out down to a radius of 0.1 nm, which is smaller than the effective radius of a water molecule. The value of porosity is then defined as

$$\phi(m) = V_{\text{pores}}(m, 0)/V(0, 0) \quad (3)$$

with V_{pores} the total volume of the inserted spheres. As suggested by Coussy,⁴⁶ we use the Lagrangian porosity, referring pore changes to the pore volume of the dry material at zero stress, $V(0, 0)$. The initial porosity at zero moisture content equals $\phi(0, 0) = \phi_0$. From this procedure, we can also determine the pore size distribution at different moisture contents, using the radius of the sphere as pore radius. We note that the porosity of the system is determined under free swelling without any mechanical constraint, i.e., $\sigma_x = \sigma_y = \sigma_z = 0$. At this point the advantage of MD becomes evident, since we can freeze easily the material in a swollen state and determine the corresponding porosity and porosity distribution by the technique described above. As an example, the pores of AC in the dry state and at saturation are depicted in Figure 2e,f, where the pores are represented as spheres without showing the polymeric skeleton.

Mechanical Tests. The mechanical measurements are carried out on the polymer systems at a sequence of moisture contents. During mechanical measurements the number of inserted water molecules is unchanged so the moduli we report are for undrained conditions. As the polymer systems were found to behave isotropically we report the bulk and shear modulus.

In order to obtain the bulk modulus at a moisture content m , a uniform stress of 100 MPa is applied. The stress value is chosen in a way such that the material remains in the linear elastic regime. A system is allowed to evolve to equilibrium, the moisture content being held at m , and the change in volume is measured. Then the bulk modulus is determined as

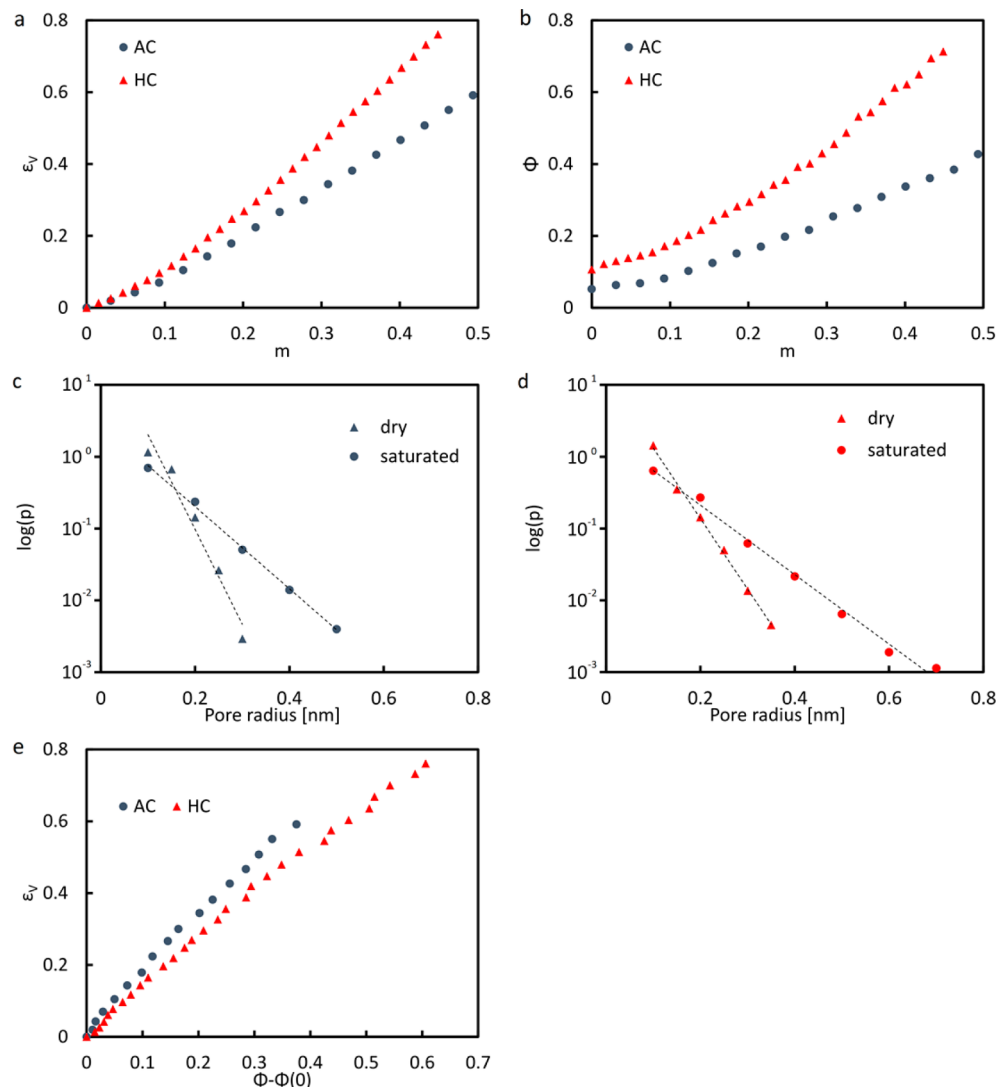


Figure 3. Moisture adsorption influencing the states of AC and HC. (a) Volumetric swelling. (b) Total porosity versus moisture content. (c, d) Pore size distribution of amorphous cellulose (c) and hemicellulose (d). Number of pores decreases exponentially. Adsorbed water increases porosity by creating new pores and increasing the radii of existing ones. (e) Volumetric swelling scales linearly with porosity change.

$$K(m) = \frac{\sigma}{\frac{V(m, \sigma) - V(m, 0)}{V(m, 0)}} \quad (4)$$

where σ is the applied stress and $V(m, \sigma)$ is the volume at moisture content m and stress σ .

The shear modulus at a given moisture content m is obtained in a triaxial test. In the x -direction a tensile stress $\sigma_x = 20$ MPa is imposed, and in the two orthogonal directions a compressive stress $\sigma_y = \sigma_z = -10$ MPa is imposed. The resulting average strain in the x -direction, ε_x , is measured. The shear modulus for an isotropic material can then be found as

$$G(m) = \frac{\sigma_x}{2\varepsilon_x(m)} \quad (5)$$

The choice of an optimal value for the stresses is a compromise. Too large stress levels can introduce a sampling beyond the elastic region. On the other hand, if the stress is not high enough, the error on the volume becomes more important due to volume fluctuations. By doing pretests, we ensured that, at the chosen stress, the system remains in the linear elastic regime and the influence of fluctuations is minimized.

The Poisson's ratio ν can be determined from K and G as

$$\nu = \nu(K, G) = \frac{3K - 2G}{6K + 2G} \quad (6)$$

Hydrogen Bonds. The existence of a hydrogen bond between a polymer sorption site and a water molecule or another OH group is determined by (1) the distance between donor and acceptor that has to be smaller than 0.35 nm and (2) the angle between hydrogen, donor, and acceptor that should not exceed 30°.⁴⁷ In a hydrated polymer, one can distinguish four types of hydrogen bonds: intrachain, interchain, polymer to water, and water to water. We study in this paper the intra- and interchain hydrogen bonds, i.e., not those formed with water molecules.

RESULTS

Swelling and Porosity Measurements. In Figure 3a, we show the volumetric strain as a function of moisture content for both AC and HC. A clear linear regime is found above $m = 0.1$. The lower slope below $m = 0.1$ has been analyzed in detail in the previous work¹⁵ and has been explained by the fact that water molecules first fill the initial porosity, resulting in less swelling. We note that the slope of HC in the second region is larger than that of AC, and we will return to this point below.

In Figure 3b, we show the porosity of AC and HC as a function of moisture content. Porosity increases with moisture content in a linear way beyond small values of moisture

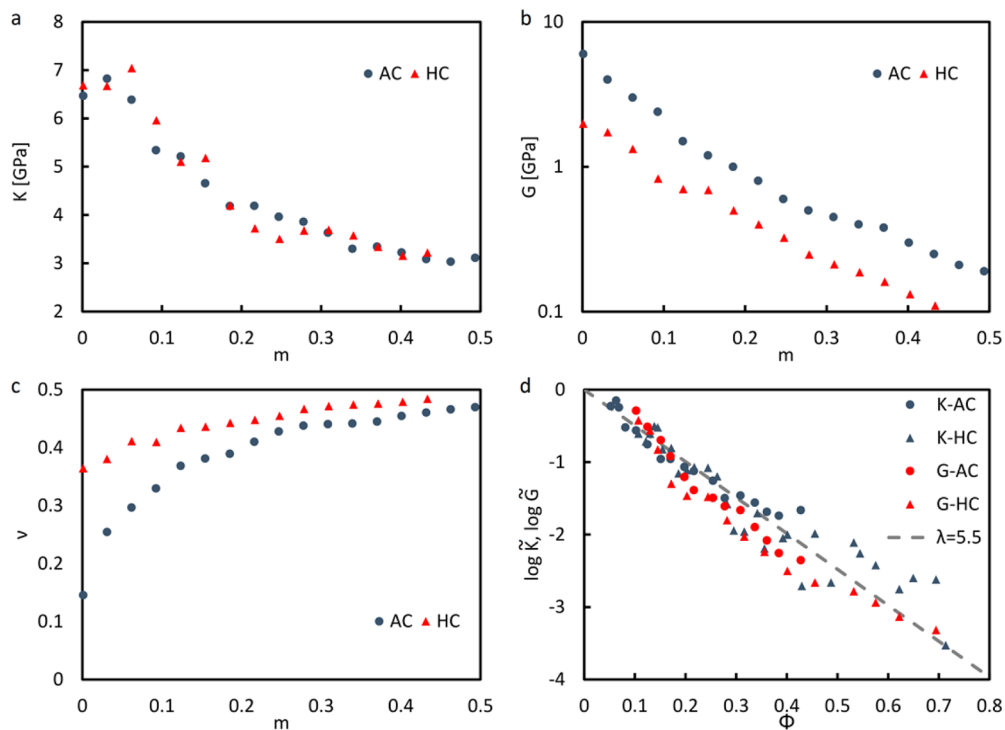


Figure 4. Moisture adsorption influencing mechanical properties of AC and HC: (a) bulk modulus, (b) shear modulus, and (d) Poisson's ratio, plotted versus moisture content. (d) Scaled bulk and shear moduli of AC and HC versus porosity show exponential scaling.

content. The initial porosity of HC is found to be larger than that of AC, which is caused mainly by their different chemical composition: HC is a branched polymer composed by three different sugars which has to deter self-packing, when compared to AC which is rather homogeneous and an easier-to-pack chain.

As we expect some structural changes as the polymers adsorb water, we analyze the pore size distribution in dry and saturated states for AC and HC. Two examples of pore arrangements are shown in Figure 2e,f. In the saturated state (Figure 2f) larger pores appear compared to the dry state (Figure 2e). Water molecules are found to push away polymer chains, allowing existing pores to grow, creating more porosity and enabling further adsorption. We show the pore size distributions in Figure 3c,d on a semilog scale. We observe that the porosity distributions follow an exponential law. Note that an exponential distribution of pore size is very commonly observed in fibrous materials and has a sound theoretical basis.^{48–50} We determined the scaling factors of the exponential distributions, $p \sim \exp(-\alpha r)$. For amorphous cellulose, the factor α is -30.4 and -13.4 nm^{-1} in the dry state and at saturation, respectively. For HC, the corresponding values are -22.6 and -11.1 nm^{-1} . In general, the smaller the factor, the wider the distribution and the larger pores are present in the pore system. Comparing the factors, we find that the larger value of porosity of HC compared to the one of AC is mainly due to the presence of larger pores in HC. This difference can be attributed to the difference in chemical composition between AC and HC as pointed out above. During further sorption the scaling factors of the pore distributions decrease, meaning the increase of total porosity is mainly accompanied by a growth of the pore size. However, we note that if water molecules were added to a material of very high stiffness, the swelling curve would not be linear, and at a certain value of

moisture content, no additional molecule could enter the system and the pore size will remain constant.

As we know the moisture content–porosity relationship (Figure 3b), we can also plot the swelling strain versus porosity change $\varphi - \varphi_0$ (Figure 3e). We find a linear relation, and moreover, the slope is almost identical for AC and HC. This means that the swelling or increase in total volume is directly related to the additional pore space created by adsorbed water molecules and that both polymers behave similarly. An explanation for this similar behavior will be given below when studying the hydrogen bond evolution.

Mechanical Measurements. In Figure 4a–c, we show the bulk modulus K , the shear modulus G , and the Poisson ratio ν as a function of the moisture content for AC and HC. In Figure 4a,b, the bulk and shear moduli decrease with moisture content, characteristic for a mechanical weakening of the material. By driving the system to the saturation point, the bulk modulus decreases roughly by a factor of 2.5. The shear modulus is found to decrease much importantly by nearly 2 orders of magnitude. Poisson's ratio (Figure 4c) is found to increase approaching a value of 0.5 at the saturation point, characteristic for a rubberlike behavior.⁵¹ While the bulk moduli of AC and HC are quite similar, HC has a smaller shear modulus and accordingly a higher Poisson's ratio than AC. An explanation will be given below.

As we know the moisture content–porosity relationship (Figure 3b), we can plot the mechanical data as a function of porosity. A power law scaling relation versus porosity is introduced for the normalized bulk and shear modulus

$$\log \tilde{K} = \log \frac{K - K_{\text{sat}}}{K_0 - K_{\text{sat}}} = -\lambda \phi \quad (7)$$

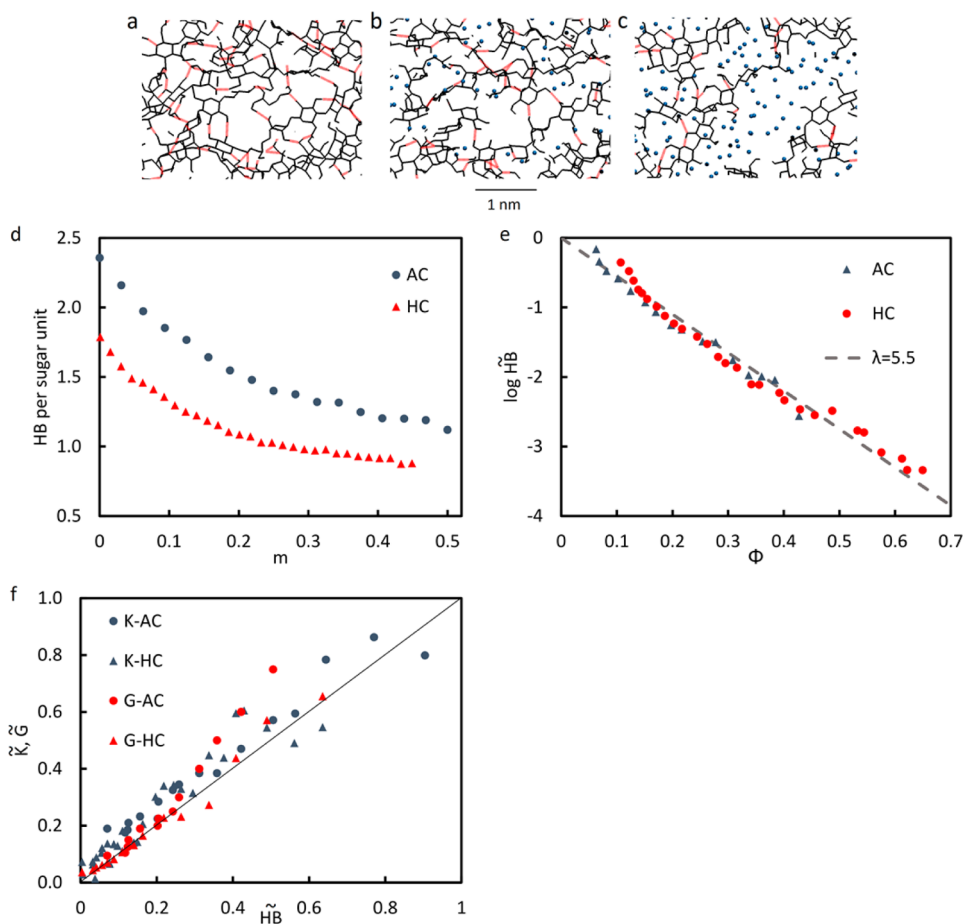


Figure 5. Illustration of hydrogen bonds breaking in a (a) dry, (b) intermediate, and (c) saturated state. Adsorbed water molecules break inter- and intrapolymeric hydrogen bonds and push the chains apart, increasing pore space. Hydrogen bonds as a function of moisture content: (d) number of AC–AC (HC–HC) bonds per total number of sugar units; (e) scaled number of hydrogen bonds as a function of porosity. (g) Scaled moduli versus scaled hydrogen bonds number prove that the bond-breaking is the main source of mechanical weakening.

$$\log \tilde{G} = \log \frac{G - G_{\text{sat}}}{G_0 - G_{\text{sat}}} = -\lambda\phi \quad (8)$$

where λ is the scaling factor and subscript “0” and “sat” denote the value in the dry state and saturation, respectively. The mechanical measurements, scaled in the manner described above, are presented in Figure 4d. We observe that, using this scaling, the K and G moduli for both polymers, AC and HC, collapse on one curve. The scaling factor λ equals approximately 5.5. The unique scaling of AC and HC versus porosity suggests that the decrease of bulk and shear modulus is caused by a similar physical process, which will be further elaborated next by studying the hydrogen bond evolution.

Hydrogen Bonds. In Figure 5a–c, we show characteristic structures of the AC polymer system in a dry, intermediate, and saturated state. In the dry state (Figure 5a), pores of different sizes exist, and the polymer chains (black lines) are interconnected by numerous polymer–polymer hydrogen bonds (red lines). Some of the hydrogen bonds are formed within a chain, e.g., between neighboring residues. When a polymer system becomes hydrated (Figure 5b), water molecules (blue dots) enter the space between the chains and by their presence initiate the breaking of interchain hydrogen bonds. This is followed by an increase of pore size and total porosity. This process continues up to saturation (Figure 5c), and finally in many places the chains become

totally disconnected, while the pores reach their maximum size (Figure 2e,f). The number of hydrogen bonds per backbone residue is presented in Figure 5d. One can notice that the breaking of polymer-to-polymer hydrogen bonds is a continuous process showing a gradual decrease. At saturation the polymer loses approximately half of its initial hydrogen bonds (Figure 5d), which means a drop from 2 or more down to 1 hydrogen bond per residue, on average.

The smaller number of hydrogen bonds in HC explains the lower shear modulus of HC compared to AC (Figure 4b), since the hydrogen bonds interconnecting different polymer chains reduce the shear deformations between them. Remarkably the smaller number of hydrogen bonds for HC does not play such an important role for the bulk stiffness, which is similar for AC and HC (Figure 4a). This is because the bulk stiffness results mainly from the volumetric compression (tension) of the total polymer structure, while the shear stiffness depends mainly on the shearing along weaker planes in the material.

The drop of the shear modulus to very low values with increasing moisture content can now be explained by the fact that, with increasing breakage of the hydrogen bonds, water fills important regions in the polymer system (Figure 2c). This means that, at very high moisture content, there exist planes where almost only the water phase is present. Since water has a zero shear stiffness, this results in the observed decrease of shear stiffness over 2 orders of magnitude. At high moisture

contents, the high breakage of hydrogen bonds and the low shear stiffness mean that the material starts to act, as mentioned above, as a rubberlike material, with a Poisson ratio reaching 0.5 (Figure 4c). For the bulk modulus we observe a smaller decrease of its value as a function of moisture content (Figure 4a). This can be explained by the fact that, in bulk compression (tension), the adsorbed water contributes with its own bulk modulus (equal to 2 GPa) to the total stiffness of the material. Although the bulk modulus of water is smaller than that of the dry polymers, the presence of water in the pores prevents the bulk modulus from a decrease of more than 1 order of magnitude, as it is in the case for the shear modulus.

We now study the scaling of the number of hydrogen bonds of AC and HC versus porosity, by introducing a hydrogen bond power law versus porosity, i.e.

$$\log \overline{HB} = \log \frac{HB - HB_{\text{sat}}}{HB_0 - HB_{\text{sat}}} = -\lambda_{HB}\phi \quad (9)$$

The plot of scaled hydrogen bonds versus porosity is given in Figure 5e. We find that the curves for AC and HC collapse on one curve showing a scaling factor of hydrogen bond loss of $\lambda_{HB} = 5.5$.

We note that the scaling factor λ_{HB} for the hydrogen bond loss has a value similar to the weakening factor for the mechanical moduli ($\lambda = 5.5$). This suggests that the loss of hydrogen bonds shows a similar rate as the mechanical weakening. This can be visualized in Figure 5f where we plot the scaled mechanical moduli versus scaled number of hydrogen bonds for both polymers, and we find an almost 1:1 relation. If we assume $\lambda = \lambda_{HB}$, one can show that

$$\frac{K(\phi) - K_{\text{sat}}}{K(\phi(0)) - K_{\text{sat}}} = \frac{G(\phi) - G_{\text{sat}}}{G(\phi(0)) - G_{\text{sat}}} = \frac{HB(\phi) - HB_{\text{sat}}}{HB(\phi(0)) - HB_{\text{sat}}} \quad (10)$$

On the basis of these results, we can conclude that hydrogen bond breakage during hydration, and the resulting increase in porosity, is the main mechanism for mechanical weakening of the material in bulk and shear behavior.

An equation of the type

$$\log(\tilde{x}(\phi)) = \log\left(\frac{x(\phi) - x_{\text{sat}}}{x_0 - x_{\text{sat}}}\right) = -\lambda\phi \quad (11)$$

with x being K , G , or HB , is a particular solution of a first-order differential equation

$$\frac{dx}{d\phi} = -\lambda(x - x_{\text{sat}}) \quad (12)$$

that has a universal meaning and drives such physical processes as heat transfer, Malthusian growth of population size, or radioactive decay. The physical understanding that accompanies this equation is that the decay in K and G is related to the exponential decay in HB , where HB decreases at a rate proportional to the current value of $HB - HB_{\text{sat}}$.

CONCLUSION

In this paper we have shown how water adsorption influences the swelling and mechanical properties of two common noncrystalline biopolymers, amorphous cellulose and galacto-glucomannan, an example of hemicellulose. We showed that, although adsorption is a complex process, it can be captured with simple scaling of the mechanical moduli and swelling to

porosity changes. Swelling shows a linear relation with porosity change. The process of weakening shows a power law scaling and can be explained by the breaking of polymer–polymer hydrogen bonds. We found a similar scaling for AC and HC showing that, for the considered polymers, their chemical composition is less important than the change of porosity. It is shown that the decay in bulk and shear stiffness follows an exponential decay, proportional to the decay in hydrogen bonds, where the number of hydrogen bonds decreases at a rate proportional to its current value (first-order differential equation). The main structural change the material undergoes is breaking of hydrogen bonds, which weakens the skeleton.

With this study we prove the usefulness of studying complex systems at the atomistic scale. Our MD results, first of all, confirm the experimentally measured softening upon absorption, linked to breaking of H-bonds. Moreover, the results introduce a detailed understanding of the evolution of mechanical properties, hydrogen bond breaking, and their interrelation. Although MD simulations are limited, mainly by time and spatial resolution, they can provide information difficult to get with other techniques, such as the relation between mechanical weakening and hydrogen bond loss or between swelling and change in porosity and pore size distribution.

AUTHOR INFORMATION

Corresponding Author

*E-mail kulasinski@arch.ethz.ch (K.K.).

Notes

The authors declare no competing financial interest.

ACKNOWLEDGMENTS

We acknowledge the fruitful discussions with Sergey Churakov, Benoit Coasne, and Koen Van den Abeele.

REFERENCES

- Moon, R. J.; Martini, A.; Laird, J.; Simonsen, J.; Youngblood, J. *Chem. Soc. Rev.* **2011**, *40* (7), 3941.
- Dinwoodie, J. M. *Timber, Its Nature and Behaviour*, 2nd ed.; E&FN Spon: London, 2000.
- Eichhorn, S. J.; Young, R. J. *Cellulose* **2001**, *8* (3), 197.
- Andersson, S.; Serimaa, R.; Paakkari, T.; Saranpaa, P.; Pesonen, E. *J. Wood Sci.* **2003**, *49* (6), 531.
- Agarwal, U. P. *Planta* **2006**, *224* (5), 1141.
- Klemm, D.; Heublein, B.; Fink, H.-P.; Bohn, A. *Angew. Chem., Int. Ed.* **2005**, *44* (22), 3358.
- Nishiyama, Y. *J. Wood Sci.* **2009**, *55* (4), 241.
- Salmén, L.; Olsson, A.-M.; Stevanic, J. S.; Radotic, K. *BioResources* **2012**, *7* (1), 521.
- Rissanen, J. V.; Gre, H.; Willfo, S.; Murzin, D. Y.; Salmi, T. *Ind. Eng. Chem. Res.* **2014**, *53*, 6341.
- Xu, C.; Lepänen, A.-S.; Eklund, P.; Holmlund, P.; Sjöholm, R.; Sundberg, K.; Willför, S. *Carbohydr. Res.* **2010**, *345* (6), 810.
- Ebringerová, A.; Hromádková, Z.; Hřibalová, V.; Xu, C.; Holmbom, B.; Sundberg, A.; Willför, S. *Int. J. Biol. Macromol.* **2008**, *42* (1), 1.
- Xu, C.; Willför, S.; Holmlund, P.; Holmbom, B. *Carbohydr. Polym.* **2009**, *75* (3), 498.
- Nishiyama, Y.; Chanzy, H.; Langan, P. *Abstr. Pap. Am. Chem. Soc.* **2002**, *223*, D26.
- Nishiyama, Y.; Langan, P.; Chanzy, H. *J. Am. Chem. Soc.* **2002**, *124* (31), 9074.
- Kulasinski, K.; Keten, S.; Churakov, S. V.; Guyer, R.; Carmeliet, J.; Derome, D. *ACS Macro Lett.* **2014**, *3*, 1037.
- Cousins, W. *J. Wood Sci. Technol.* **1978**, *12* (3), 161.

- (17) Salmen, L. *C. R. Biol.* **2004**, *327* (9–10), 873.
- (18) Engelund, E. T.; Thygesen, L. G.; Svensson, S.; Hill, C. A. S. *Wood Sci. Technol.* **2013**, *47* (1), 141.
- (19) Tremblay, C.; Cloutier, A.; Fortin, Y. *Wood Sci. Technol.* **2000**, *34* (2), 109.
- (20) Tremblay, C.; Cloutier, A.; Fortin, Y. *Wood Sci. Technol.* **2000**, *34* (3), 253.
- (21) Sonderegger, W.; Vecellio, M.; Zwicker, P.; Niemz, P. *Holzforschung* **2011**, *65* (6), 819.
- (22) Araujo, C. D.; Avramidis, S.; MacKay, A. L. *Holzforschung* **1994**, *48* (1), 69.
- (23) Charlier, L.; Mazeau, K. *J. Phys. Chem. B* **2012**, *116* (14), 4163.
- (24) Mazeau, K.; Heux, L. *J. Phys. Chem. B* **2003**, *107* (10), 2394.
- (25) Liao, R.; Zhu, M.; Zhou, X.; Zhang, F.; Yan, J.; Zhu, W.; Gu, C. *Mod. Phys. Lett. B* **2012**, *26* (14), 1250088.
- (26) Liao, R. J.; Zhu, M. Z.; Zhou, X.; Zhang, F. Z.; Yan, J. M.; Zhu, W. B.; Gu, C. *Mod. Phys. Lett. B* **2012**, *26* (14).
- (27) Chen, W.; Wang, T.; Lickfield, G. C. *J. Polym. Sci., Part B: Polym. Phys.* **2007**, *45* (14), 1821.
- (28) Chen, W.; Lickfield, G. C.; Yang, C. Q. *Polymer* **2004**, *45* (21), 7357.
- (29) Chen, W.; Lickfield, G. C.; Yang, C. Q. *Polymer* **2004**, *45* (3), 1063.
- (30) Zhang, X.; Tschoopp, M. A.; Horstemeyer, M. F.; Shi, S. Q.; Cao, J. *Int. J. Model. Identif. Control* **2013**, *18* (3), 211.
- (31) Bocahut, A.; Delannoy, J.-Y.; Vergelati, C.; Mazeau, K. *Cellulose* **2014**, *21*, 3897.
- (32) Mazeau, K.; Moine, C.; Krausz, P.; Gloaguen, V. *Carbohydr. Res.* **2005**, *340* (18), 2752.
- (33) Zhang, Q.; Brumer, H.; Ågren, H.; Tu, Y. *Carbohydr. Res.* **2011**, *346* (16), 2595.
- (34) Peri, S.; Karim, M. N.; Khare, R. *Carbohydr. Res.* **2011**, *346* (6), 867.
- (35) Salmen, L.; Burgert, I. *Holzforschung* **2009**, *63* (2), 121.
- (36) Olsson, A.-M.; Salmén, L.; Eder, M.; Burgert, I. *Wood Sci. Technol.* **2006**, *41* (1), 59.
- (37) Hess, B.; Kutzner, C.; van der Spoel, D.; Lindahl, E. *J. Chem. Theory Comput.* **2008**, *4* (3), 435.
- (38) Oostenbrink, C.; Villa, A.; Mark, A. E.; Van Gunsteren, W. F. *J. Comput. Chem.* **2004**, *25* (13), 1656.
- (39) Lins, R. D.; Hünenberger, P. H. *J. Comput. Chem.* **2005**, *26* (13), 1400.
- (40) Bussi, G.; Donadio, D.; Parrinello, M. *J. Chem. Phys.* **2007**, *126* (1), 014101.
- (41) Berendsen, H. J. C.; Postma, J. P. M.; van Gunsteren, W. F.; DiNola, A.; Haak, J. R. *J. Chem. Phys.* **1984**, *81* (8), 3684.
- (42) Gomes, T. C. F.; Skaf, M. S. *J. Comput. Chem.* **2012**, *33* (14), 1338.
- (43) Kulasinski, K.; Keten, S.; Churakov, S. V.; Derome, D.; Carmeliet, J. *Cellulose* **2014**, *21* (3), 1103.
- (44) Smith, P. E.; van Gunsteren, W. F. *J. Chem. Phys.* **1994**, *100* (4), 3169.
- (45) Derome, D.; Rafsanjani, A.; Patera, A.; Guyer, R.; Carmeliet, J. *Philos. Mag.* **2012**, *92* (28–30), 3680.
- (46) Coussy, O. *Int. J. Numer. Anal. Meth. Geomech.* **2007**, *31* (March), 1675.
- (47) Apol, E.; Apostolov, R.; Berendsen, H. J. C.; Van Buuren, A.; Bjelkmar, P.; Van Drunen, R.; Feenstra, A.; Groenhof, G.; Kasson, P.; Larsson, P. R. *Inst. Technol. Uppsala Univ. Stock. Uppsala, Sweden*, 2010.
- (48) Hellén, E. K. O.; Alava, M. J.; Niskanen, K. *J. Appl. Phys.* **1997**, *81*, 6425.
- (49) Niskanen, K.; Rajatora, H. *J. Pulp Pap. Sci.* **2002**, *28* (7), 228.
- (50) Nesbakk, T.; Helle, T. *J. Pulp Pap. Sci.* **2002**, *28* (12), 406.
- (51) Browning, C. E.; Husman, G. E.; Whitney, J. M. *ASTM STP 1977*, *617*, 481.